Macromolecules

ARTICLE

pubs.acs.org/Macromolecules

Chain Dynamics of Unentangled Poly(ethylene-*alt*-propylene) Melts by Means of Neutron Scattering and Fully Atomistic Molecular Dynamics Simulations

R. Pérez-Aparicio,[*,†] F. Alvarez,[†,‡] A. Arbe,[‡] L. Willner,[⊥] D. Richter,[⊥] P. Falus,[§] and J. Colmenero[†,‡,∥]

[†]Departamento de Física de Materiales UPV/EHU, Apartado 1072, 20080 San Sebastián, Spain

[‡]Centro de Física de Materiales (CSIC−UPV/EHU), Materials Physics Center (MPC), Paseo Manuel de Lardizabal 5, 20018 San Sebastián, Spain

[⊥]Institut für Festkörperforschung, Forschungszentrum Jülich GmbH, D−52425 Jülich, Germany

[§]Institut Laue Langevin, BP 156, 38042 Grenoble Cedex 9, France

[∥]Donostia International Physics Center, Paseo Manuel de Lardizabal 4, 20018 San Sebastián, Spain

ABSTRACT: We have studied the chain dynamics of poly(ethylene-*alt*-propylene) by combining neutron spin echo experiments and fully atomistic molecular dynamics simulations. We have focused on molecular weights of the order of two times the entanglement mass, for which, in principle, the topological constraints are not important and the chain dynamics should be well described in terms of the Rouse model. From the comparison between experimental and simulated results we have validated our simulation cell. We have checked the predictions of the Rouse model on both sets of data and compared the resulting relevant parameters with those obtained from other experimental works in the literature. Moreover, taking advantage of the validated simulated system we have calculated directly the Rouse modes and correlators to investigate the limitations of the model extending the study at lower temperatures. We have found deviations from Rouse behavior at short length scales that can be attributed to the local potentials and a sublinear increase of the mean squared displacement of the chain center of mass with time, probably originating from intermolecular interactions.

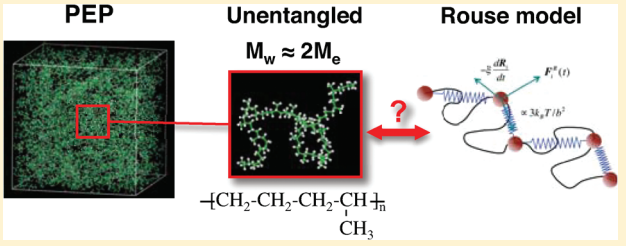

INTRODUCTION

Polymers may adopt a huge number of conformations determined by the relative positions of their monomers, which depend on the intra- and interchain interactions. At length scales much larger than the monomer size, the chemical details can be ignored in the description of the chain dynamics and polymer melts show unique dynamic processes that are controlled by the chain connectivity and the molecular weight of the macromolecules. These processes ultimately determine the rheological properties of polymer melts, which have been extensively studied by mechanical relaxation techniques. With the development of neutron scattering (NS) techniques, in particular of neutron spin echo (NSE), it has also become possible to investigate the chain dynamics at a molecular level. These techniques allow accessing hydrogen motions in protonated samples and the single chain dynamic structure factor in blends of protonated and deuterated chains, such that theoretical models can be directly contrasted. The standard model for polymer chain dynamics in the melt, the so-called Rouse model,[1] considers the conformational entropy as the only source for restoring forces which stabilizes excursions from equilibrium. Because of the difficulty of obtaining rheological data on unentangled chains in the melt[2,3] the validity of the Rouse model has been mainly proven by dielectric spectroscopy on type-A polymers (i.e., with a dipole component parallel to the main chain) (see, e.g., refs 4 and 5) and by NS on different polymers.[6] From a conceptual point of view, this model has limitations: (i) at large distances, where long chain melt topological constraints cause entanglements leading to the reptation mechanism, and (ii) at shorter distances, where the simplifying assumptions cease to be valid and the local chain structure and dynamics comes into play. Locally the chain is stiff; furthermore, as a consequence of the rotational potentials, local relaxation mechanisms through the rotational barriers also start to play a role. At length scales of the order of the intermolecular distances, we approach the regime of the α process and more locally possible secondary relaxations. An intriguing question in polymer physics is how does the crossover from Rouse to segmental dynamics take place. One of the key ingredients to answer this question would be to know when the Rouse model ceases to be valid. This is not an obvious issue, since NS results might be described in terms of this model even at momentum transfers[7] and times[8] where the model should be, in principle, unrealistic. Recently, a number of NS investigations on different polymers (polyisobutylene (PIB),[9] poly(vinyl ethylene)

Received: December 20, 2010
Revised: March 3, 2011
Published: March 30, 2011

(PVE),[10] poly(dimethylsiloxane) (PDMS)[11]) have tried to determine the limits for applicability of the Rouse model. The role of the intramolecular barriers was put forward in the study of PIB,[9] that showed much more pronounced deviations from Rouse than the extremely flexible PDMS. However, the uncertainties involved in the experiments and the impossibility to directly access the Rouse correlators prevent a thorough analysis of the sources for Rouse deviations.

It has been extensively proved that the combination of atomistic molecular dynamics (MD) simulations with NS experiments provides a very useful tool for investigating the structure and dynamics of polymer melts at local and intermolecular scales, i.e., where these systems display universal features of glass forming liquids (see refs 6 and 12−14 as recent representative references). Current computing capabilities even allow building big enough cells to address the chain dynamics in unentangled polymer systems with atomistic detail. Starting from a properly validated simulation cell, it is possible to rely on computed magnitudes that cannot be accessed experimentally, like mean squared displacements,[15] or perform a Rouse mode analysis. This kind of methodology can thus shed light also on the problem of the limits of applicability of the Rouse model in homopolymers. Recent examples of this synergy can be found applied to polybutadiene (PB),[16] polyethylene (PE),[17] or poly(ethylene oxide) (PEO).[18]

Here we present a study of the chain dynamics in poly(ethylene-*alt*-propylene) (PEP) melts by means of NS and fully atomistic MD simulations for low molecular weights ($M_w \sim 2M_e$, where M_e is the entanglement mass). For these chain lengths, the entanglement effects that limit the validity of the Rouse model at large length scales are negligible. By NSE we have covered a momentum-transfer Q range between 0.03 and 0.25 Å^{-1}. The investigated temperature was 492 K in order to ensure the decay of the correlation functions in the Q and t range of the experimental window. The good agreement found from the comparison between the experimental and simulated results has allowed validating our simulated system. Furthermore, we have checked the predictions of the Rouse model on these sets of data and compared them with other experimental results on PEP from the literature. Taking advantage of the validated simulated system, we have calculated directly the Rouse modes and other correlators to investigate the limitations of the model in this relatively simple polymer. The deviations and limits found for PEP Rouse-like dynamics are discussed in comparison with results previously reported for other polymers, mainly PIB[9] and PEO.[18] The impact of these deviations on the experimentally accessible dynamic structure factors (reciprocal space) is finally discussed.

EXPERIMENTS

Samples. The sample investigated in this work was a blend of protonated (h-PEP) and deuterated (d-PEP) chains of poly(ethylene-*alt*-propylene): 30% h-PEP/70% d-PEP, $M_w \approx 6$ kg/mol. The mixture was accomplished just by stirring the two components for some time in a cuvette. The niobium sample container was filled with the mixture in a glovebox under argon and closed also there. The two PEP polymers, h-PEP6k and d-PEP6k, were synthesized by anionic polymerization of isoprene-h_8 and isoprene-d_8 and subsequent saturation with H_2 and D_2, respectively. The two PI-precursor materials were polymerized with *t*-butyllithium as initiator in benzene. Deuterated isoprene monomer was prepared from acetylene and acetone-d_6 following largely the method of Krebs et al.[19] The degree of deuteration of the isoprene-d_8 was determined to be 94%. The saturation to the PEP polymers was accomplished by means of a conventional Pd/$BaSO_4$ catalyst at 4 MPa H_2/D_2 pressure and 100°C in *n*-heptane. The number-average molecular weight, M_n, of the h-PI6k precursor was determined by ^{1}H NMR in deuterochloroform using the 9 protons of the *t*-butyl initiator group as internal reference. Both PI polymers were characterized by size exclusion chromatography (SEC) in THF with a PL-GPC220 chromatograph from Polymer Laboratories, Varian, equipped with a refractive index detector and a set of 3 PLgel 5 μm mixed D columns. The molecular weight distribution, M_w/M_n, was determined relative to polystyrene standards. The elution volumes of both polymers are almost identical. The number-average molecular weight, M_n, of the d-PI6k was calculated according to: $M_n(\text{d-PI6k}) = (M(\text{d-PI6k})/M(\text{h-PI6k}))_{(PS-cal)}$ $(75.5/68)$ $M_n(\text{h-PI6k})_{NMR}$, where the first term represents the ratio of molecular weights obtained by SEC with PS-calibration, while the second term denotes the ratio of the molecular weights of the repeat units of isoprene-d_8 (94%D) and isoprene-h_8, respectively, multiplied with the M_n of h-PI6k obtained by ^{1}H NMR. After saturation the resulting PEP materials were remeasured by SEC. No change in the molecular weight distribution could be observed. The molecular weights were corrected for the addition of H_2 and D_2, respectively. The characteristics of both PEP materials, h-PEP6k and d-PEP6k, are summarized in Table1.

Table 1. Molecular Weight Characteristics of h-PEP6k and d-PEP6k

polymer	M_n (kg/mol)	M_w/M_n
h-PEP6k	6.2	1.02
d-PEP6k	6.85	1.02

Neutron Spin Echo. NSE is the neutron scattering technique that offers the highest energy resolution. In addition, NSE is unique in that it accesses the intermediate scattering functions directly in the time domain. This is achieved by the direct observation of the velocity change of the neutron in the scattering process encoding the neutron energy transfer into its spin rotation.[20] In this way, the application of precession magnetic fields before and after the scattering event results in a polarization of the neutron that depends only on the velocity difference of each neutron individually, irrespective of its initial velocity. Energy resolution and monochromization of the incident beam are decoupled, and resolutions in energy of the order of $\Delta E/E \approx 10^{-5}$ can be achieved with an incident neutron spectrum of 20% bandwidth. These experiments access the following normalized combination of coherent and incoherent scattering intensities

$$I_{NSE}(Q,t) = \frac{I_{coh}(Q,t) - \frac{1}{3}I_{inc}(Q,t)}{I_{coh}(Q,0) - \frac{1}{3}I_{inc}(Q,0)} \quad (1)$$

where Q is the momentum transfer that depends on the neutron wavelength λ and the scattering angle θ [$Q = (4\pi/\lambda)\sin(\theta/2)$].

In this work we performed NSE experiments at the IN15 instrument (Institut Laue-Langevin, ILL, Grenoble, France), which offers a resolution $\Delta\lambda/\lambda = 15\%$. With $\lambda = 22$ Å we could gain access to Q values of 0.03, 0.05, and 0.077 Å^{-1}; with $\lambda = 14.5$ Å to 0.115 Å^{-1}; and with $\lambda = 10$ and 6.3 Å to 0.25 Å^{-1}. The accessed Fourier times covered a range from 0.05 up to 500 ns. The sample was put in a flat niobium holder with 2.5 *mm* of thickness. The temperature of the experiment was 492 K and the measuring time per angle was about 7 h for λ = 22 Å and about 4 h for the other wavelengths. Direct deconvolution of the measured spectra from the experimental resolution was carried out dividing by the measurement of a graphite sample at room temperature. The scattering from the deuterated matrix was subtracted by using the measurement on

Table 2. Details of the Simulated Cells

T (K)	ρ_{exp} (g/cm^3)	ρ_{MDS} (g/cm^3)	cell dimension (Å)
492		0.7447	53.155
413	0.79	0.7948	52.014
350		0.8266	51.338
300	0.856	0.8549	50.766

a fully deuterated d-PEP sample ($M_w \approx 200$ kg/mol, $M_w/M_n \approx 1.02$[21]) of 1 mm thickness at the same conditions. In the subtraction, the relative value of the sample transmissions ($T_{h-PEP/d-PEP}/T_{d-PEP} = 0.57/0.93$) and the concentration were taken into account, yielding finally the corrected function $I^{corr}_{NSE}(Q,t)$. In the blend investigated, the main contribution to the scattering signal comes from the coherent scattering arising from the contrast between the protonated chains and the deuterated matrix ($\Delta\rho^2 = 5.01 \times 10^{21}$ cm^{-4}). For the chains investigated, the coherent differential cross section due to this contrast amounts to $d\Sigma/d\Omega = 13.79P(Q)$ cm^{-1} ($P(Q)$: chain form factor), while the incoherent contribution is $d\Sigma_{inc}/d\Omega = 0.16$ cm^{-1}. For $Q \lesssim 0.077$ Å^{-1}, the absolute value of the relative incoherent contribution to the NSE signal is $\lesssim$1% and $I_{NSE} \simeq S_{chain}(Q,t)/S_{chain}(Q,0)$. This value increases to 2% at $Q = 0.115$ Å^{-1} and $\approx$10% at the highest Q investigated. We note that the correction procedure above-described does not eliminate this incoherent contribution from the signal.

MOLECULAR DYNAMICS SIMULATIONS

The fully atomistic MD simulations were carried out by using the *Materials Studio* and the *DISCOVER* module from *Accelrys* with the *COMPASS Force Field* (Condensed-phase Optimized Molecular Potentials for Atomistic Simulation Studies). The *COMPASS* force field has been parametrized and validated using condensed-phase properties in addition to various *ab initio* and empirical data for molecules. Therefore, this forcefield enables accurate and simultaneous prediction of structural, conformational, vibrational, and thermophysical properties, that exist for a broad range of isolated molecules and in condensed phases, and under a wide range of conditions of temperature and pressure.[22−28] The model cubic cell was built by means of the *Amorphous Cell Protocol*, originally proposed by Theodorou and Suter.[29,30]

In this work we started from a system composed of 12 different well equilibrated chains of 80 monomers each (M_w = 5.6 kg/mol), being 14424 atoms in total, and we constructed a cubic cell with periodic boundary conditions at 413 *K* and an initial density set to 0.79 g/cm^3, which is the experimental value at that temperature[31] (Table 2). Standard minimization procedures (Polak−Ribière conjugate gradients method) were applied to the constructed cell in order to minimize the so obtained energy structure. Furthermore, a *NVT* dynamics (constant number of atoms, volume and temperature) of 1 ns was run to equilibrate the amorphous cell at 413 *K*. The equilibrium density of the cell was achieved by running *NPT* dynamics (constant number of atoms, pressure and temperature in the cell) at fixed atmospheric pressure (P = 0.0001 GPa) . After three runs of 1 ns we reached a density of 0.7948 g/cm^3 (close to the experimental value and to the average over the runs), that leads to a cell dimension of 52.014 Å of side. Further simulations were carried out in the *NVT* ensemble at 413 K. As integration method, the velocity−Verlet algorithm with a time step of 1 fs has been used. For temperature control instead of a real temperature-bath coupling (i.e., Nosé−Hoover thermostat) we have followed a velocity scaling procedure but with a wide temperature window of 10 *K*, where greater temperature fluctuations are allowed but the trajectory is disturbed less. In fact, we have checked in a similar polymeric system that by following this simple procedure we obtain similar results to those obtained with a *NVE* ensemble (constant total energy instead of temperature), which has the proper Newtonian dynamics.[32] The system so obtained was used as a starting point for collecting data during successive molecular dynamics runs of 1, 2, and 100 ns. Data were collected every 0.01, 0.05, and 0.5 ps, respectively. Finally, an extra run of 1 ns was executed in order to check the possible appearance of aging process but nearly indistinguishable results were obtained from the consecutive simulation runs, confirming equilibration of the sample.

The so-obtained system was used to generate corresponding cells at other temperatures namely, 492, 350, and 300 K. In order to do this, *NPT* simulation runs of some nanoseconds (depending on the temperature) were used to readapt the system to each new temperature, allowing the size of the system to rearrange itself in order to accommodate to the new density at each temperature. In this way, we got the values displayed in Table 2 for the cell sizes and densities. Subsequent *NVT* runs of 1 ns were performed for equilibration at each temperature before collecting data for analysis, in the same way as above-described for 413 K.

In a previous work,[21] the results from these fully atomistic simulations have been carefully validated by comparison with NS experiments in the similar dynamic range on fully deuterated and fully protonated PEP samples. From the atomic trajectories obtained during the simulation runs the magnitudes measured by NS (diffraction with polarization analysis and NSE) were calculated and directly compared with the experimental data. The good agreement found validated the results concerning the short-range order and the dynamical features (collective and H self-motions) at intra- and intermolecular level, i.e., where the segmental (α)-relaxation is the dominant process. We have to note that in order to achieve a perfect matching of the characteristic times obtained from experiments and simulations for the α-relaxation a shift by a factor of 2 had to be applied to the time scale (simulations are slower).

THE ROUSE MODEL: SCATTERING FROM A ROUSE CHAIN

The dynamics of medium length chains can be described in terms of the Rouse model,[1,33] that considers a Gaussian chain representing a coarse-grained polymer model of beads connected by entropic springs. The model focuses on length scales $b < R < R_{ee}$, where b is the statistical segment and R_{ee} is the average end to end distance of the chain ($R_{ee}^2 = Nb^2$, with N the number of beads in the chain). The contribution of the surrounding chains is assumed to be a stochastic background, as well as to create a friction characterized by the friction coefficient ξ. The resulting Langevin equation can be solved by transforming to the normal coordinates (Rouse modes)

$$\mathbf{X}_p(t) = \frac{1}{N}\sum_{i=1}^{N} \mathbf{R}_i(t) \cos\left[\frac{p\pi}{N}\left(i - \frac{1}{2}\right)\right] \qquad (2)$$

with p the mode number (p = 0, 1, 2, 3, ..., $N - 1$). The zeroth mode gives the position of the center of mass (CoM) of the chain and the others are associated with internal motions of the chain with a "wavelength" of the order of N/p. The Rouse correlations,

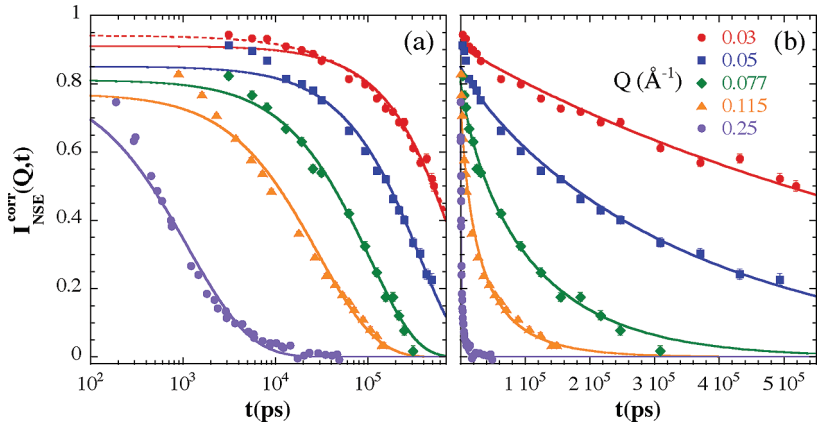

Figure 1. Time dependence of the NSE signal obtained from the sample 30% h-PEP/70% d-PEP ($M_w \approx 6$ kg/mol) and corrected for matrix scattering (symbols) at the specified Q values and 492 K: (a) logarithmic time scale and (b) linear time scale. The solid lines are fits with the Rouse model (eq 9), where the remaining incoherent contribution has also been considered. The dashed line in part a is a KWW description of the lowest-Q data, where the β-value has been fixed to 0.8.

with amplitudes

$$\langle X_p^2(0)\rangle = \frac{b^2}{8N}\sin^{-2}\left(\frac{\pi p}{2N}\right) \tag{3}$$

relax independently and exponentially:

$$\langle \mathbf{X}_p(t)\cdot\mathbf{X}_p(0)\rangle/\langle X_p^2(0)\rangle = \exp(-t/\tau_p) \tag{4}$$

Here τ_p is the characteristic relaxation time of the mode p

$$\tau_p^{-1} = 4W\sin^2\left(\frac{p\pi}{2N}\right) \tag{5}$$

with the Rouse time $\tau_R = \tau_{p=1}$. The Rouse frequency W is given by

$$W = \frac{3k_BT}{\xi b^2} \tag{6}$$

The correlator of the CoM of the Rouse chain is always proportional to time:

$$\langle \mathbf{X}_0(t)\cdot\mathbf{X}_0(0)\rangle = \frac{6k_BT}{N\xi}t \tag{7}$$

with an associated diffusion coefficient:

$$D = \frac{Wb^4}{3Nb^2} = \frac{Wb^4}{3R_{ee}^2} \tag{8}$$

In the Rouse model, the coherent dynamic structure factor of a single chain (accessible on h-/d-labeled samples) can be written as

$$S_{chain}(Q,t) = \frac{1}{N}\exp[-Q^2Dt]\sum_{n=1}^{N}\sum_{m=1}^{N}\exp\left[-\frac{Q^2b^2}{6}|n-m|\right] \times \exp\left\{-\frac{2}{3}\frac{R_{ee}^2Q^2}{\pi^2}\sum_{p=1}^{N}\frac{1}{p^2}\left[\cos\left(\frac{p\pi m}{N}\right)\cos\left(\frac{p\pi n}{N}\right)\left(1-\exp\left(-\frac{tp^2}{\tau_R}\right)\right)\right]\right\} \tag{9}$$

where for $QR_{ee} > 1$ and $t < \tau_R$ the internal relaxations dominate, and for $QR_{ee} < 1$ $S_{chain}(Q,t)$ reveals the CoM diffusion of the chain. On the other hand, the self-correlation function accessible on protonated samples is calculated on the basis of the Gaussian approximation, that relates $S_{inc}(Q,t)$ directly to the mean squared displacement of the scattering centers $\langle r^2(t)\rangle = 2((Wb^4)/(\pi))^{1/2}t^{1/2}+6Dt$:

$$S_{inc}(Q,t) = \exp[-Q^2Dt]\exp\left[-\left(\frac{Wb^4Q^4t}{9\pi}\right)^{1/2}\right] \tag{10}$$

For Q values where the diffusion contribution is not important, eq 10 has just the form of a stretched exponential or Kohlrausch–Williams–Watts (KWW) function

$$\Phi_{KWW} = \exp\left[-\left(\frac{t}{\tau^{KWW}}\right)^{\beta}\right] \tag{11}$$

with a shape parameter $\beta = 0.5$ and a characteristic time

$$\tau_{self}^{KWW}(Q) = \frac{9\pi}{Wb^4}Q^{-4} \tag{12}$$

Thus, NS experiments on either protonated or labeled samples provide direct microscopic access to Wb^4. We will use this variable to characterize the dynamics in the Rouse regime in both, simulated and experimental systems. Obviously, Wb^4 is not Q-dependent in the Rouse model and it depends on the molecular weight of the chains only for short chains.

RESULTS

Neutron Scattering Results. The results from the IN15 experiment $I_{NSE}^{corr}(Q,t)$ are shown in Figure 1 both, in linear and logarithmic scales for the time axis to highlight the long and short time behavior, respectively. The results were fitted by using the Rouse expression for $S_{chain}(Q,t)$ of eq 9, where the diffusion effects are included. The residual incoherent contribution to the NSE signal (described also in terms of the Rouse model) was also included in the fitting function. As mentioned above, this contribution is only noticeable in the highest Q value here investigated. The model prediction was found to lay always above the experimental data, evidencing the need to include

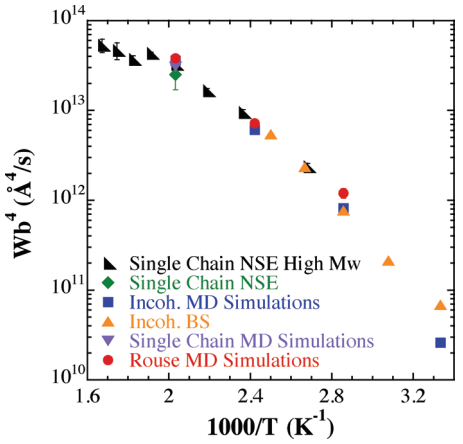

Figure 2. Temperature dependence of the characteristic Rouse variable Wb^4 for PEP: from NSE experiments on a PEP sample of $M_w \approx 80$ kg/mol (right triangles) from the short-time regime published in ref 35, and on the 30% h-PEP/70% d-PEP ($M_w \approx 6$ kg/mol) (diamond); from the study of the self-motions of hydrogens by means of atomistic MD simulations (M_w = 5.6 kg/mol) (squares) and backscattering experiments on a fully protonated sample ($M_w \approx 20$ kg/mol; ref 36) (triangles); from the single chain dynamics calculated from the atomistic simulations (inverted triangle); and finally, from the Rouse mode analysis performed from the atomistic simulations (full circles). Shift in the simulation results has been applied in order to compare with experiments (see text).

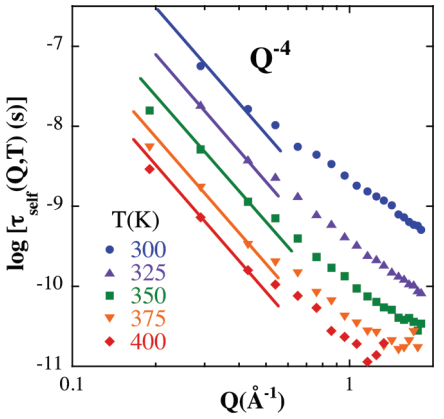

Figure 3. Momentum transfer dependence of the characteristic times obtained for the incoherent scattering function of PEP hydrogens by means of backscattering experiments (see ref 36) at the different temperatures investigated: 300 (circles), 350 (squares), and 400 K (diamonds). The solid lines display the power law $\tau_{self}(Q,T) \propto Q^{-4}$.

prefactors accounting for amplitudes smaller than 1 in the fitting curves. The fitting parameters were thus these amplitudes and the Rouse variable Wb^4. The value of R_{ee} needed for these fits was estimated from experimental results (small angle NS experiments) on the ratio between the unperturbed mean squared end-to-end distance and the molar mass ${R_{ee_0}}^2/M$ published in refs 34 and 35 that characterizes the chain dimensions. This ratio is constant for relatively large molecular weights, where the Gaussian statistics is well fulfilled. For our system such relation would not be completely right, but it can be used as a good approximation. The estimated value of R_{ee} was 68 Å at 492 *K*. The fits presented in Figure 1 were done considering *D* as predicted by the Rouse model, i.e., depending on Wb^4 by means of eq 8. The model function represents well the data in the linear representation (Figure 1b), though some discrepancies can be envisaged at short times in the logarithmic-time representation (Figure 1a). From these fits the value of Wb^4 was extracted. Since this variable depends on molecular weight only for very short chains, it is possible to perform a direct comparison between experimental results on different samples. In Figure 2 we compare the obtained value with those corresponding to the short-time regime (to avoid effects of reptation) of the single chain dynamic structure factor of a PEP sample of $M_w \approx 80$ kg/mol from ref 35. Furthermore, Wb^4 can also be estimated from the incoherent scattering measured by means of backscattering experiments on a fully protonated sample addressing the self-motions of hydrogens, which has already been published in ref 36. Those data were phenomenologically described in terms of a KWW functional form (eq 11) with $\beta = 0.5$, and the resulting characteristic times are represented in Figure 3. In that sample, the chains were quite long ($M_w \approx 20$ kg/mol) and translational diffusion contributed there only marginally. Thus, the scattering function of eq 10 without considering the diffusion term was implicitly used for the data description. Moreover, below $Q \approx 0.4$ Å^{-1} the *Q* dependence of the characteristic times (Figure 3) obeys the Q^{-4}-law predicted in the Rouse model (eq 12). In view of these observations, the Rouse model seems to be applicable in this range and from the characteristic times presented in Figure 3 it is possible to calculate Wb^4 by means of eq 12. The values so obtained are also presented in Figure 2. A good overlap is observed with the other results. We note that at lower temperatures the determination of Wb^4 is subject to higher uncertainties, since there the quasielastic broadening cannot be properly resolved for the lowest *Q* value. Nevertheless, the comparison among all data is very good, indicating that the chain dynamics in PEP as observed by NS on different samples and experiments is consistently described by the Rouse model within the experimental uncertainties.

Comparison between NS and MD Simulations. From the atomic trajectories collected from MD simulations—extensively validated at the intermolecular scale by NS experiments already published in ref 21—we have calculated the NSE signal (eq 1) by simulating the experimental conditions mentioned above. Thus, from the simulated system (M_w = 5.6 kg/mol) we have considered 4 protonated and 8 deuterated chains, which approximately corresponds to 33% h-PEP/66% d-PEP (close to the composition of the real sample). The deuteration level of the real chains is approximately 94% due to the remaining protonated initiator which is needed in the chain synthesis. In our simulations, this effect was not considered and the chains were treated as if they were fully deuterated. However, the slightly lower ratio of deuterated chains in the simulated system can compensate for the protonated initiator effect present in the experimental sample. Therefore, even though the scattering contrast is not exactly the same, the simulated results can be considered to be a good approximation to the measured function. Figure 4 shows the comparison of $I_{NSE}(Q,t)$ between NSE experiments and atomistic MD simulations for the two higher *Q* values measured at 492 *K*. Since from the simulations all the scattering contributions of the blend of chains were taken into account, the experimental data have been presented without subtracting the scattering from the deuterated matrix—which is necessary to isolate the pure $S_{chain}(Q,t)/S_{chain}(Q)$ (see neutron spin echo section), as done in the results presented in Figure 1. In the comparison of Figure 4, we have applied the time shift (factor of 2) needed to match the times of the α-relaxation[21] as was explained

before. The agreement is rather good regarding both, the spectral shape and the Q dependence. We have to take into account that the low Q limit in our atomistic MD simulations results from the limitations in the pair correlation calculations given by the cell size L ($r_{max} = L/2$): $Q = 2\pi/r_{max} = 4\pi/L(492\ K) \approx 0.24\ Å^{-1}$. Thus, although we find a very good agreement at $Q = 0.115\ Å^{-1}$, this function is out of the Q limit and the uncertainty in the calculation could be high. Nevertheless, the good agreement seems to confirm the validity of the simulated system—at least in the length scales covered by the simulations. Moreover, the consistency with the previous results on the local dynamics is demonstrated.

Next, the intermediate incoherent scattering function of protons $S^H_{inc}(Q,t)$ (investigated by backscattering in ref 36) was calculated from the atomic trajectories and fitted by eq 10 with D as in eq 8. Figure 5 shows the results of such fits at $Q = 0.3\ Å^{-1}$ at the investigated temperatures. The Wb^4 obtained values (the only free parameter in the fits) are also included in Figure 2 after correcting them from the time shift in the MD simulations results described above. They show an excellent agreement with the experimentally deduced values.

Finally, we have directly calculated the "pure" $S_{chain}(Q,t)$ considering only correlations involving atoms from a given individual chain. In this calculation, the periodic boundary conditions have been released so that the global Cartesian coordinates of the molecule are considered. These coordinates are not restricted to the cell size. Despite this fact, in any dynamics the cell size is an underlying limiting factor. We have calculated $S_{chain}(Q,t)$ at the same Q values as in the NSE experiments and fitted them with the expression for the Rouse model (eq 9). Figure 6 shows the fits in linear and logarithmic scales of the time axis. The fits do not describe properly the correlation functions at short times, in a similar way as it is observed in the logarithmic-time representation of the experimental data (Figure 1a). The Wb^4 values obtained are presented in Figure 2, showing a consistent comparison with the other results once they have been properly corrected by the above-mentioned factor 2.

From all these observations, we can conclude that the simulated system behaves as the real one also concerning chain dynamics and that the Rouse model seems to reasonably describe such dynamics.

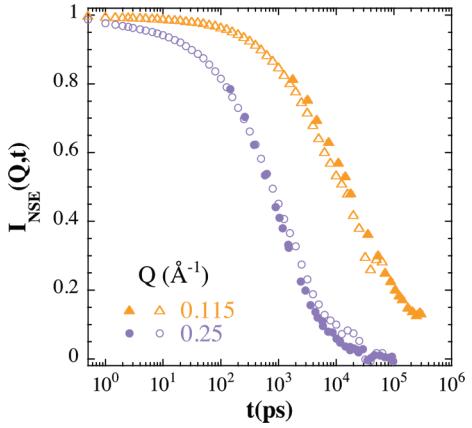

Figure 4. Time dependence of the signal measured by NSE in the sample 30% h-PEP/70% d-PEP ($M_w \approx 6$ kg/mol) (full symbols) and computed from atomistic MD simulations ($M_w = 5.6$ kg/mol) (empty symbols) at the specified Q values and 492 K. Shift in the experimental time scales has been applied in order to match both sets of data (see text).

EXPLOITING THE SIMULATIONS. ROUSE MODE ANALYSIS

After this validation, we can take advantage of the simulations in order to accurately investigate the Rouse model limits. For

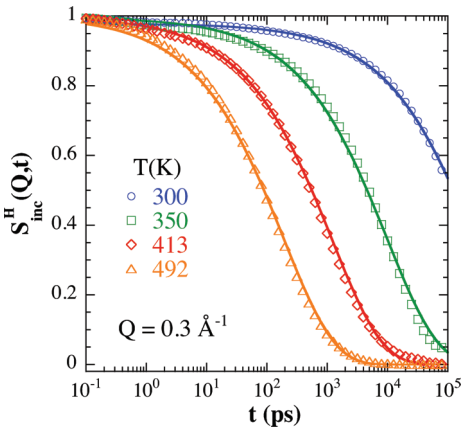

Figure 5. Time dependence of the simulated intermediate incoherent scattering function of the self-motion of hydrogens at $Q = 0.3\ Å^{-1}$ and the temperatures investigated: 300, 350, 413, and 492 K. Solid lines correspond to Rouse model fits by using eq 10.

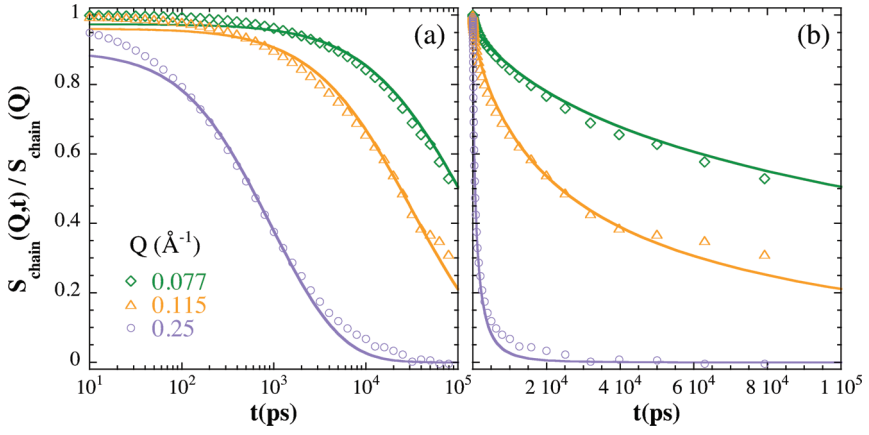

Figure 6. Single chain coherent dynamic structure factor calculated from our atomistic MD simulations at 492 K: (a) logarithmic time scale and (b) linear time scale. The solid lines are fits with the Rouse model (eq 9).

dx.doi.org/10.1021/ma102909r |*Macromolecules* 2011, 44, 3129–3139

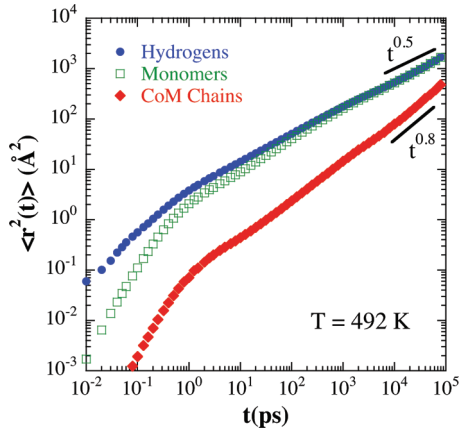

Figure 7. Time dependence of the msd of the hydrogen atoms (circles), the monomers (squares), and the CoM of the atomistic simulated chains (diamonds) at 492 K.

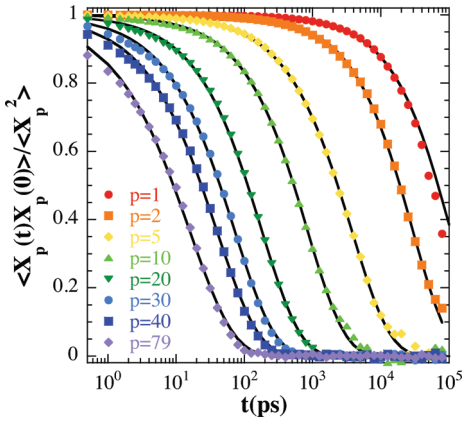

Figure 8. Normalized Rouse correlators for the indicated modes using one monomer as one bead at 492 K. The solid lines show fits by a stretched exponential function.

instance, we can calculate the atomic and the CoM mean squared displacements (msd), which cannot be directly measured by experiments. After the decageing regime, a sublinear regime is observed in the msd displacement of the hydrogens which is characteristic for glass-forming polymer dynamics. This regime is attributed to the segmental dynamics in the α-relaxation regime with a msd $\langle r^2(t)\rangle \propto t^{\beta}$, being β the stretching exponent ($0.4 \leq \beta \leq 0.6$).[37−39] Since polymers are interconnected objects with large conformational entropy, the universal entropy-driven Rouse dynamics prevails at intermediate scales. Thus, the sublinear regime following the decageing process leads to Rouse motion at larger scales and longer times, with $\langle r^2(t)\rangle \propto t^{1/2}$. This behavior is a clear signature of the Rouse motion and has been observed in simulations[18] and some NS experiments.[8,10] The hydrogen msd of simulated PEP at 492 K shows an almost direct crossover from the microscopic regime toward the Rouse-like behavior (Figure 7). NS experiments on a high molecular weight PEP melt ($M_w \approx 80$ kg/mol) published in ref 40 also present Rouse-like behavior at the same temperature. However, we also observe deviations from Rouse behavior: at times shorter than the Rouse time ($\tau_R(492\ K) = 106\ ns$) the msd of the chain CoM $\langle r_{CoM}{}^2(t)\rangle$ does not increase linearly with time. An analogous behavior has also been observed in experimental and simulation works on PB,[16] PE,[17] or PEO.[18] The time dependence of $\langle r_{CoM}{}^2(t)\rangle$ can be (at least effectively) described by a power law $\langle r_{CoM}{}^2(t)\rangle \propto t^x$ with $x < 1$, indicative for sublinear diffusion, that has generally been interpreted in terms of the effect of intermolecular interactions ignored in the Rouse model. For instance, in the mode coupling approach of Guenza[41] the solution of the corresponding generalized Langevin equation for short chains gives values of x in the range 0.85−0.97. Another possible description of the deviations of $\langle r_{CoM}{}^2(t)\rangle$ from purely diffusive behavior is provided by the mode coupling theory (MCT), if a coupling between chain dynamics and the mean surrounding medium is considered.[42] In this framework, in addition to the Rouse linear increase a contribution proportional to $t^{0.75}$ would be present, giving rise to a "globally apparent" $\langle r_{CoM}{}^2(t)\rangle \propto t^x$. Our data would be compatible with both kinds of frameworks.

Next, we perform a direct analysis of the Rouse modes and Rouse correlators $\langle \boldsymbol{X}_p(t)\cdot\boldsymbol{X}_p(0)\rangle/\langle X_p{}^2(0)\rangle$ coarse graining the atomistic MD simulations. We have defined a bead as the CoM of one monomer creating 12 chains with $N = 80$ beads each and with 80 associated modes ($p = 0, 1, ..., 79$). The chosen definition of bead is justified since the msd of the monomers is very close to that of the hydrogen atoms, at least in the interesting sublinear regime, at large time scales, as it is shown in Figure 7. Some of the normalized Rouse correlators at 492 *K* are presented in Figure 8. To check the exponentiality of the Rouse correlators (eq 4), we have fitted them by means of KWW functions (eq 11):

$$\langle \mathbf{X}_p(t)\cdot\mathbf{X}_p(0)\rangle/\langle \mathbf{X}_p^2(0)\rangle = \exp\left[-\left(t/\tau_p^{KWW}\right)^{\beta_p}\right] \qquad (13)$$

where the relaxation time τ_p^{KWW} and the stretching parameter β_p—measuring the deviations from an exponential decay—depend on mode number p. Because of bad statistics at low temperatures we considered $T \geq 350$ K. The resulting values of β_p are shown in Figure 9a as a function of the scaling variable N/p ("mode wavelength"). At high N/p values, $N/p \gtrsim 5$, β_p seems to reach a more or less constant value about 0.8−0.85 (for the highest temperatures investigated; at 350 K the results in this region are not reliable). On the other hand, for low N/p values a clearly nonexponential behavior is observed, that becomes more pronounced with decreasing temperature. Nonexponential relaxation of Rouse modes has also been reported for other systems and different simulation methods as well. For example, simulations of polymers on a lattice with uncrossability constraints,[43] atomistic MD simulations of PE and PB (see, e.g., refs 44 and 45), and more recently PEO.[18] Such deviations have been reported from theoretical treatments as well (see, e.g., refs 46 and 47). Because β_p changes for the different modes and temperatures, we have considered the average relaxation times $\langle\tau_p\rangle$ [$\langle\tau_p\rangle = \tau_p^{KWW}\beta^{-1}\Gamma(\beta^{-1})$], as characteristic for the relaxation times of the Rouse modes. The effective Rouse frequency, W^{eff}, can be calculated from $\langle\tau_p\rangle$ by means of eq 5. Both parameters, shown in Figure 9b and Figure 9c, display a clear temperature dependence and follow Rouse-like behavior (solid lines in figures) for $N/p \gtrsim 5$ or $p \lesssim 16$. There, W^{eff} tends to a constant plateau, W_0^{eff}. At shorter N/p values clear deviations from the Rouse predictions are observed. A similar trend is shown by the amplitudes of the Rouse correlators $\langle X_p{}^2(0)\rangle$ (Figure 9d). In the short N/p range, the amplitudes overlap and are massively suppressed, indicating significantly stronger restoring forces than those originating from the entropic potential of the Rouse model.

An "effective" statistical segment $(b^{eff})^2$ can be independently determined from the amplitudes of the Rouse modes according

dx.doi.org/10.1021/ma102909r |*Macromolecules* 2011, 44, 3129–3139

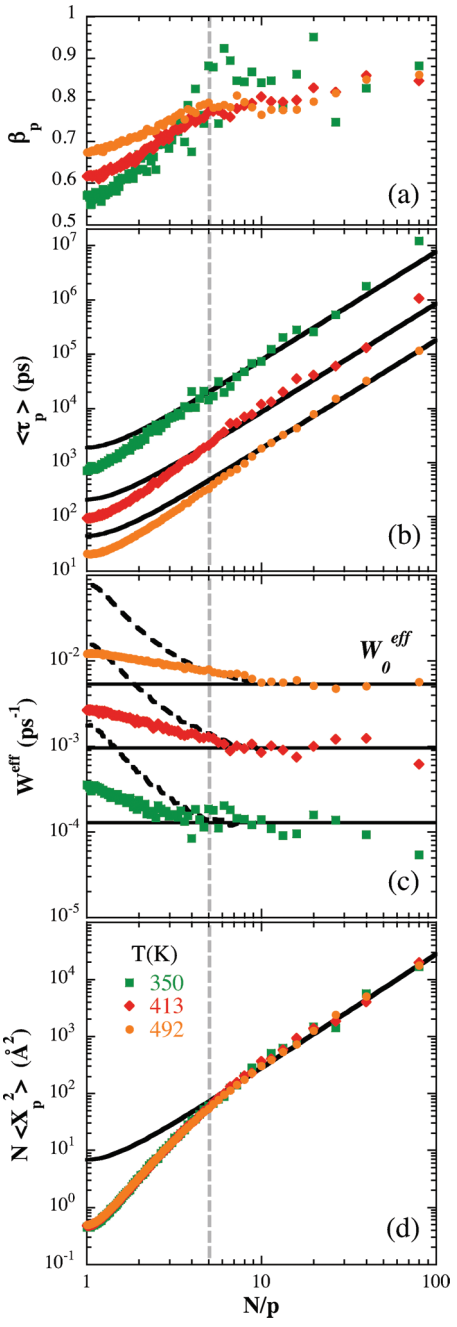

Figure 9. Parameters from Rouse model analysis as a function of N/p and the three different temperatures investigated. (a) Stretching parameters and (b) average relaxation times from KWW analysis of the Rouse correlators. (c) Rouse frequencies obtained from eq 5 and (d) amplitudes of Rouse correlators. In all figures, the vertical dashed line indicates the deviations from the Rouse model at $N/p \lesssim 5$. The solid lines in parts b−d correspond to Rouse model fits and dashed lines in part c to the expectation in the framework of the ARS model.

to eq 3, resulting in the values shown in Figure 10 as a function of N/p at the different temperatures. The mode-number dependence of $(b^{eff})^2$ reflects deviations from ideal chain statistics due to the local potentials of the atomistic system, in particular the angular potential which introduces some stiffness. These stiffness effects are more important at smaller length scales. Only at $N/p \gtrsim 10$ a constant value of $(b_0^{eff})^2 \simeq 60$ Å^2 is reached, which

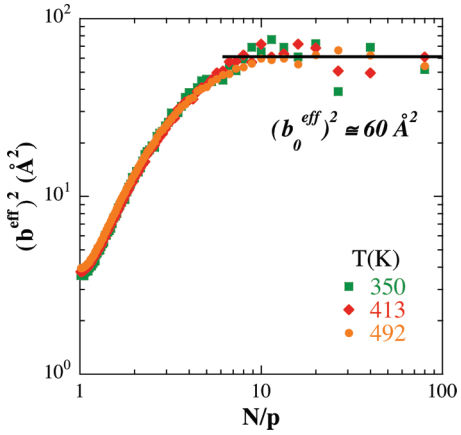

Figure 10. $(b^{eff})^2$ as a function of the scaling variable N/p for the different investigated temperatures: 350 (squares), 413 (diamonds), and 492 K (circles).

corresponds to $b_0^{eff} \simeq 7.75$ Å for the statistical segment. This value is smaller than the Kuhn statistical segment length, $b_K(492\ K) \simeq 11.2$ Å, estimated from the results published in ref 31.

To check whether the local stiffness is the only reason for the deviations of the chain *dynamics* from the Rouse behavior in the low-N/p range, we can invoke the so-called all rotational state (ARS) model.[48] In this framework, the stiffness of the chain at local scales translates in an increase of the spring constant ($3k_BT/b^2$). Accordingly, we have calculated W^{eff} by the Rouse model (eq 6) but taking $(b^{eff})^2(N/p)$ as deduced from the amplitudes (Figure 10) and fixing the friction ξ from the high N/p values of W^{eff}, W_0^{eff}, where Rouse-like behavior ($W^{eff} \sim$ constant) seems to apply. The results obtained (dashed lines in Figure 9c) evidence that the consideration of local stiffness overestimates the deviations from the Rouse model at low N/p values.

The last results suggest to postulate a mode-dependent effective friction ξ^{eff} as the responsible mechanism. These ξ^{eff} were calculated by means of eq 6 as

$$\xi^{eff}(N/p) = \frac{3k_BT}{W^{eff}(b^{eff})^2} \qquad (14)$$

where W^{eff} and $(b^{eff})^2$ depend on N/p (Figure 9c and Figure 10). Figure 11 shows the results so obtained, which decrease with increasing N/p, reaching a constant plateau ξ_0^{eff} at $N/p \gtrsim 8$. Similar behavior was observed in atomistic MD simulations on PEO melts.[18] A direct comparison between PEP and those PEO results is made in Figure 11, showing that the similarity is not only qualitative but also quantitative. In both cases the friction starts deviating from the constant limit ξ_0^{eff} at approximately the same value of the variable N/p, and the relative increase of the effective friction in going toward high-p values is nearly the same. Furthermore, qualitatively similar effects were observed in experimental works in PIB melts[9] and solutions,[11] and were interpreted in terms of an internal viscosity effect proposed by Allegra and Ganazzoli.[49] However, for PIB the mode damping effect starts from lower modes. This quantitative difference may result from the stronger rotational potentials in PIB, causing very different internal viscosities.

Thus, considering long wavelength modes $N/p \gtrsim 8$ ($p \lesssim 10$) the apparent friction and statistical segment are approximately constant and the Rouse variable defined in this limit, $W_0^{eff}(b_0^{eff})^4$, agrees very well with the compilation of Figure 2 (after applying

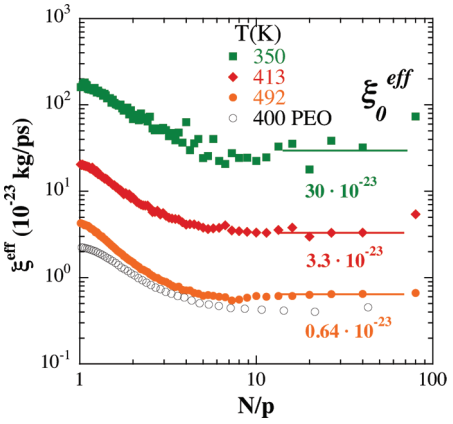

Figure 11. Effective friction ξ^{eff} as a function of the scaling variable N/p at the different investigated temperatures: 350 (squares), 413 (diamonds), and 492 K (circles). The empty symbols correspond to this parameter obtained from a similar analysis in the case of PEO[18] at 400 K (see text).

the shift accounting that simulations are a factor of 2 slower). Only the more localized modes present significant deviations from the Rouse model. The question arises: how do these localized modes affect the scattering function that is experimentally accessed? The contribution of the normal modes to $S_{chain}(Q,t)$ strongly depends on the Q value considered, but, since the dynamic structure factor is not simply broken down into a sum or product of more contributions, the Q dependence is not easy to represent. In order to make the effects more transparent, we consider the maximum possible contribution of a given mode p to the relaxation of $S_{chain}(Q,t)$. This maximum contribution is reached when the correlator $\langle \mathbf{X}_p(t)\cdot\mathbf{X}_p(0)\rangle$ has fallen to zero. We thus define the contribution factor:

$$R_p(Q) = \frac{1}{S_{chain}(Q,t=0)} \sum_{n,m=1}^{N} \exp\left[-\frac{Q^2 b^2}{6}|n-m| - \frac{2}{3}\frac{R_{ee}{}^2 Q^2}{\pi^2}\frac{1}{p^2}\cos\left(\frac{p\pi m}{N}\right)\cos\left(\frac{p\pi n}{N}\right)\right] \quad (15)$$

that describes to what extent a mode "p" may relax $S_{chain}(Q,t)$ in the limit of long times ($t \rightarrow \infty$) and under the premise that all the other modes are not active, i. e., setting in eq 9 the term $[1 - \exp(-ts^2/\tau_R) = 1$ if $s = p$ and equal to 0 otherwise. Figure 12 shows the Q dependence of the mode contribution factors for the PEP chains investigated in this work. At the lowest Q investigated, 0.03 Å^{-1}, the contributions of all the internal modes are negligible and the decay of $S_{chain}(Q,t)$ is practically due to translational diffusion. We note that at this Q value the experimental data appear to be more stretched than the Rouse description (Figure 1). This supports a sublinear increase of $\langle r_{CoM}{}^2(t)\rangle$, as that observed in the simulated system. In fact, a KWW function with $\beta = 0.8$, i. e., the exponent in the asymptotic power-law description of $\langle r_{CoM}{}^2(t)\rangle$ of the atomistic simulated chains (Figure 7), provides a better description of these data (see dashed line in Figure 1a). With increasing Q (e.g., for the next Q investigated $Q = 0.05$ Å^{-1}), the first mode starts to play a role. If Q is further increased, higher relaxation modes also begin to influence the dynamic structure factor. In fact, the largest Q here studied, 0.25 Å^{-1}, would be appreciably affected by modes higher than the 10th, where the deviations from Rouse become evident.

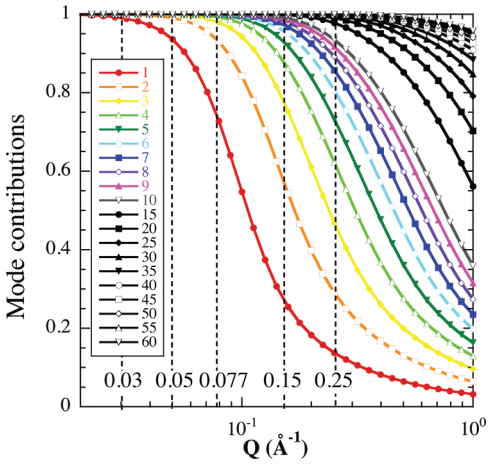

Figure 12. Q dependence of the contributions of the different modes indicated to the relaxation of the dynamic structure factor in the Rouse model. The PEP parameters of the real chains have been used in the calculation. Vertical dotted lines show the Q values investigated in the NSE experiments.

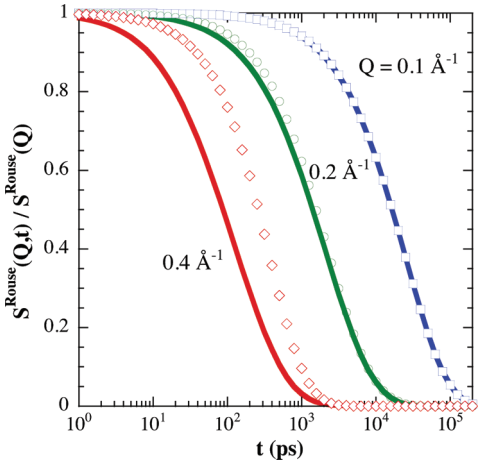

Figure 13. Single chain dynamic structure factor predicted by the Rouse model (eq 9) at the three Q values indicated (solid lines). The symbols represent the result of considering only the first 10 modes in the summation. In the calculation, the value of $W_0^{eff}(b_0^{eff})^4$ obtained for PEP at 492 K has been considered and all functions have been normalized to their respective values at $t = 0$.

Thus, we would expect that the observed deviations from Rouse would be patent in the experimental data around this Q and larger values. We note that the higher the mode number, the faster is its contribution to the total decay of $S_{chain}(Q,t)$ (see Figure 8). Therefore, the deviations arising from the high-p modes will mainly affect the short-time regime of the scattering function. To realize about the maximum deviations expected, we have calculated the difference between considering the contributions of all Rouse modes and of the 10 first modes to the Rouse dynamic structure factor in eq 9 (see Figure 13). For $Q \lesssim 0.2$ Å^{-1} the decay is almost completely determined by the ten first modes, where $W^{eff}(b^{eff})^4$ is constant. As above commented, the incipient deviations detectable at $Q = 0.2$ Å^{-1} are most evident in the short-time regime. At a higher Q like $Q = 0.4$ Å^{-1}, modes higher than ten substantially contribute to the decay. In the extreme case where

dx.doi.org/10.1021/ma102909r |*Macromolecules* 2011, 44, 3129–3139

these modes were completely frozen, the observed decay would correspond to the symbols, while perfect Rouse would deliver the line. Deviations as those found in the simulations would produce something in between. Thus, we could say that at $Q \approx 0.4$ Å^{-1} and above we could expect clear deviations from pure Rouse behavior in the experiments. This value is consistent with the results on the self-motions depicted in Figure 3. If the results for the characteristic times above $Q \approx 0.4$ Å^{-1} are considered, deviations from the Q^{-4} dependence become apparent and a fit to eq 12 would deliver a value of the effective Rouse variable smaller than the right one —compatible with a damping of the dynamics.

We note that the deviations from Rouse dynamics found at short times in Figure 1 and Figure 6 can also be partially due to the fact that the model simply does not include any dynamical process related to the microscopic dynamics (e.g., vibrations) that are present in real and fully atomistic samples. The allowed prefactors in the Rouse fits would overcome this problem if the characteristic times of the neglected fast processes are well separated (much faster) than the relaxation times characteristic for Rouse dynamics. Then, a Debye—Waller-like factor should provide a good parametrization of the additional fast dynamics. The observation of larger experimental/simulated values than the Rouse predictions affected by prefactors suggests that some of the faster additional processes occur at time scales intermediate between the microscopic (picosecond) regime and the region where Rouse starts to dominate the dynamics.

We finally comment on a somewhat paradoxical situation that could be found at first sight in the comparison between PEP and PEO limits for validity of the Rouse model. Despite the quantitative similarity of the deviations from Rouse behavior in both polymers demonstrated above (Figure 11), for PEO a substantially larger limiting Q value (≈ 0.6 Å^{-1}) for applicability of the Rouse model has been reported.[18] This apparent discrepancy arises from the different value of the statistical segment in both polymers. From the corresponding simulations, for PEP we obtain $b_0 \approx 7.75$ Å and for PEO, $b_0 \approx 5$ Å. The same N/p-value for deviations from Rouse behavior for both polymers implies a much larger corresponding p-number for PEO, that translates in a higher Q value for observing the deviations in the dynamic structure factor.

CONCLUSIONS

The single chain dynamic structure factor of PEP obtained from both NSE and atomistic MD simulations could be reasonably well described in terms of the Rouse model and in a consistent way with previous literature results. The Rouse mode analysis of the simulation data has shown deviations from Rouse behavior for all the investigated temperatures in the short length scale, even when the chain-stiffness is considered in the model through an ARS-like approach. Such deviations can be addressed in terms of a mode-number (length scale) dependent effective friction coefficient which decreases with the length scale reaching a constant value (pure Rouse) at $N/p \gtrsim 8$. These results underline the role of the local potentials in the chain dynamics of polymers. The experimentally accessed functions reflect these effects at high Q values and mainly short times. In addition, they are also affected by faster processes that are not considered in the Rouse model. Moreover, below τ_R, $\langle r_{CoM}{}^2(t)\rangle$ increases *sublinearly* with time, presumably due to the effect of intermolecular interactions neglected in the Rouse model. This is reflected in a stretching of $S_{chain}(Q,t)$ at low Q, where it is dominated by translational diffusion.

AUTHOR INFORMATION

Corresponding Author
E-mail: rperezaparicio@gmail.es.

ACKNOWLEDGMENT

We thank M. Monkenbusch and R. Lund for their help with neutron data evaluation. We thank support by the "Donostia International Physics Center", the European Commission NoE SoftComp, Contract NMP3-CT-2004-502235, FP7-PEOPLE-2007-1-1-ITN (DYNACOP, EU), the projects MAT2007-63681, IT-436-07 (GV) and the Spanish Ministerio de Educacion y Ciencia (Grant No. CSD2006-53). R.P.A. acknowledges Grant BES-2005-10794 (MAT2004-01017).

REFERENCES

(1) Rouse, P. E. *J. Chem. Phys.* **1953**, *21* (7), 1272.
(2) Ferry, J. D. *Viscoelastic Properties of Polymers*; Wiley: New York, 1970.
(3) McLeish, T. C. B. *Adv. Phys.* **2002**, *51*, 1379.
(4) Watanabe, H.; Urakawa, O.; Yamada, H.; Yao, M.-L. *Macromolecules* **1996**, *29*, 755.
(5) Riedel, C.; Alegría, A.; Tordjeman, P.; Colmenero, J. *Macromolecules* **2009**, *42*, 8492.
(6) Richter, D.; Monkenbusch, M.; Arbe, A.; Colmenero, J. *Neutron Spin Echo in Polymer Systems*; Advances in Polymer Science 174; Springer-Verlag: Berlin, 2005.
(7) Allen, G.; Higgings, J. S.; Macounachie, A.; Ghosh, R. E. *Chem. Soc. Faraday Trans. 2* **1982**, *78*, 2117.
(8) Arbe, A.; Colmenero, J. *Phys. Rev. E* **2009**, *80*, 041805.
(9) Richter, D.; Monkenbusch, M.; Allgaier, J.; Arbe, A.; Colmenero, J.; Farago, B.; Cheol Bae, Y.; Faust, R. *J. Chem. Phys.* **1999**, *111*, 6107.
(10) Richter, D.; Monkenbusch, M.; Willner, L.; Arbe, A.; Colmenero, J.; Farago, B. *Europhys. Lett.* **2004**, *66*, 239.
(11) Arbe, A.; Monkenbusch, M.; Stellbrink, J.; Richter, D.; Farago, B.; Almdal, K.; Faust, R. *Macromolecules* **2001**, *34*, 1281.
(12) Narros, A.; Arbe, A.; Alvarez, F.; Colmenero, J.; Richter, D. *J. Chem. Phys.* **2008**, *128*, 224905.
(13) Genix, A.-C.; Arbe, A.; Alvarez, F.; Colmenero, J.; Willner, L.; Richter, D. *Phys. Rev. E* **2005**, *72*, 031808.
(14) Ahumada, O.; Theodorou, D. N.; Triolo, A.; Arrighi, V.; Karatasos, C.; Ryckaert, J.-P. *Macromolecules* **2002**, *35*, 7110.
(15) We note that NS accesses the incoherent scattering function in the reciprocal space. To extract mean squared displacements from NS experiments, the Gaussian approximation is usually invoked, although it is rarely fulfilled.
(16) Smith, G. D.; Paul, W.; Monkenbusch, M.; Willner, L.; Richter, D.; Qiu, X. H.; Ediger, M. D. *Macromolecules* **1999**, *32*, 8857.
(17) Zamponi, M.; Wischnewski, A.; Monkenbusch, M.; Willner, L.; Richter, D.; Falus, P.; Farago, B.; Guenza, M. G. *J. Phys. Chem. B* **2008**, *112*, 16220.
(18) Brodeck, M.; Alvarez, F.; Arbe, A.; Juranyi, F.; Unruh, T.; Holderer, O.; Colmenero, J.; Richter, D. *J. Chem. Phys.* **2009**, *130*, 094908.
(19) Krebs, F. C.; Jorgensen, M.; Lebech, B.; Almdal, K.; Pedersen, W. B. *Polym. Bull.* **2000**, *43*, 485.
(20) Mezei, F. *Neutron Spin Echo, Lecture Notes in Physics*; Springer-Verlag: Heidelberg, Germany, 1980; Vol. 28.
(21) Pérez-Aparicio, R.; Arbe, A.; Alvarez, F.; Colmenero, J.; Willner, L. *Macromolecules* **2009**, *42*, 8271.
(22) Sun, H.; Rigby, D. *Spectrochim. Acta* **1997**, *A153*, 1301.
(23) Rigby, D.; Sun, H.; Eichinger, B. E. *Polym. Int.* **1997**, *44*, 311.
(24) Sun, H. *J. Phys. Chem. B* **1998**, *102*, 7338.

(25) Sun, H.; Ren, P.; Fried, J. R. *Comput. Theor. Polymer Sci.* **1998**, *8*, 229.
(26) Bunte, S. W.; Sun, H. *J. Phys. Chem. B* **2000**, *104*, 2477.
(27) Yang, J.; Ren, Y.; Tian, A.; Sun, H. *J. Phys. Chem. B* **2000**, *104*, 4951.
(28) McQuaid, M. J.; Sun, H.; Rigby, D. *J. Comput. Chem.* **2004**, *25*, 61.
(29) Theodorou, D. N.; Suter, U. W. *Macromolecules* **1985**, *18*, 1467.
(30) Theodorou, D. N.; Suter, U. W. *Macromolecules* **1986**, *19*, 379.
(31) Fetters, L. J.; Lohse, D. J.; Colby, R. H. In *Physical Properties of Polymers Handbook*, 2nd ed.; Mark, J. E., Ed.; Springer: New York, 2007; Chapter 25.
(32) Colmenero, J.; Alvarez, F.; Arbe, A. *Phys. Rev. E* **2002**, *65*, 041804.
(33) Doi, M.; Edwards, S. F. *The Theory of Polymer Dynamics*: Oxford University; Oxford, England, 1986.
(34) Fetters, L. J.; Lohse, D. J.; Richter, D.; Witten, T. A.; Zirkel, A. *Macromolecules* **1994**, *27*, 4639.
(35) Richter, D.; Farago, B.; Butera, R.; Fetters, L. J.; Huang, J. S.; Ewen, B. *Macromolecules* **1993**, *26*, 795.
(36) Pérez-Aparicio, R.; Arbe, A.; Colmenero, J.; Frick, B.; Willner, L.; Richter, D.; Fetters, L. J. *Macromolecules* **2006**, *39*, 1060.
(37) Colmenero, J.; Alegría, A.; Arbe, A.; Frick, B. *Phys. Rev. Lett.* **1992**, *69*, 478.
(38) Arbe, A.; Colmenero, J.; Monkenbusch, M.; Richter, D. *Phys. Rev. Lett.* **1998**, *81*, 590.
(39) Farago, B.; Arbe, A.; Colmenero, J.; Faust, R.; Buchenau, U.; Richter, D. *Phys. Rev. E* **2002**, *65*, 051803.
(40) Wischnewski, A.; Monkenbusch, M.; Willner, L.; Richter, D.; Farago, B.; Kali, G. *Phys. Rev. Lett.* **2003**, *90*, 058302.
(41) Guenza, M. *J. Chem. Phys.* **1999**, *110*, 7574.
(42) Baschnagel, J. Private communication.
(43) Shaffer, J. S. *J. Chem. Phys.* **1995**, *103*, 761.
(44) Paul, W.; Smith, G. D.; Yoon, D. Y.; Farago, B.; Rathegeber, S.; Zirkel, A.; Willner, L.; Richter, D. *Phys. Rev. Lett.* **1998**, *80*, 2346.
(45) Smith, G. D.; Paul, W.; Monkenbusch, M.; Richter, D. *Chem. Phys.* **2000**, *261*, 61.
(46) Guenza, M. *Phys. Rev. Lett.* **2002**, *88*, 025901.
(47) Schweizer, K. S. *J. Chem. Phys.* **1989**, *91*, 5802.
(48) Brückner, S. *Macromolecules* **1981**, *14*, 449.
(49) Allegra, G.; Ganazzoli, F. *Macromolecules* **1981**, *14*, 1110.